The 4th International Conference
"Advanced Composite Materials Engineering "
COMAT 2012
18- 20 October 2012, Brasov, Romania

ON THE SONIC COMPOSITE VISUALIZATION WITH HAPTIC INTERFACES

V. Chiroiu[1], Cornel Brişan[2], Ş. Donescu[3], L. Munteanu[4]
[1]Institute of Solid Mechanics, veturiachiroiu@yahoo.com
[2]Technical University of Cluj-Napoca, Cornel.Brisan@mmfm.utcluj.ro
[3]Technical University of Civil Engineering, stefania.donescu@yahoo.com
[4]Institute of Solid Mechanics, ligia_munteanu@hotmail.com

Abstract: *A model for the virtual reality system configuration using a haptic interface for physically manipulation in order to display tactual information to the user is introduced in this paper. The idea is to have a correct visual feedback of the interface and to use it in controlling the transition between the atomistic and continuum regions for the sonic composites.*
Keywords: *Haptics, Sonic composite, Full band-gap.*

1. INTRODUCTION

A sonic composite is a 3D finite size array composed of scatterers embedded into the matrix. The scatterers are local resonators which scater, diffuse or disperse energy, such as spheres, bars, chains of various geometries made of functionally graded, piezoelectric materials, steel or other materials [1]. Figure 1 shows a scatterer made of carbon nanotube rope segments. Figure 1 shows such a carbon nanotube rope made from 6 subropes, each subrope being composed from 7 groups of single wall carbon nanotubes. Each group contains 25 carbon nanotubes with two different radii (zigzag and armchair 6.26A, h = 0.617A and 16.33A, h = 0.998A), and the core group consists of 49 chiral carbon nanotube with the same radius (3.22A and h = 0.6A), into a polymeric matrix [1, 2]

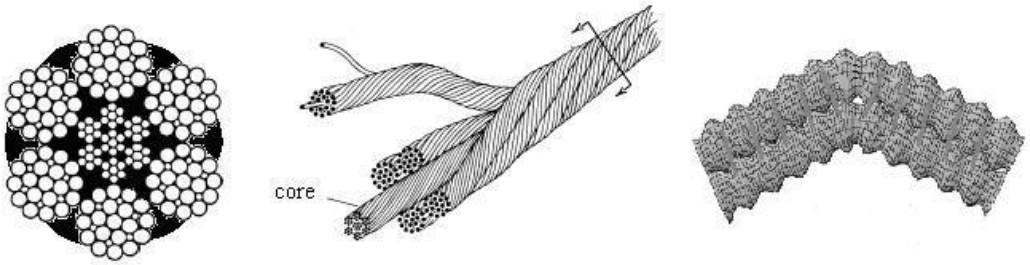

Figure 1. Scatterer made of carbon nanotube nanoropes [1, 2].

The sonic compositer is a sonic version of a photonic crystal and is architectured such that the sound is not allowed to propagate in certain full band-gaps due to complete reflections. We must add that commercially available sound absorbing materials cannot selectively attenuate sound in a desired frequency band. The design and understanding of new architectures of such materials as scatterers have many applications such as acoustic filters, sonic panels, sound shields, transducers, acoustic wave guides for stopping of noise and vibrations in closed spaces (especially for achieving the acoustic comfort control in engineering and applied aeronautics).
The haptic technologies provide new tools to grow the human capacity to manipulate the matter in order to create new materials with desired properties. Haptic interfaces are devices that can be applied for manual interaction of matter with the virtual environments or tele-operated remote systems [3, 4]. The transition or boundary region between the atomistic and continuum regions can be manipulated via the haptic visualization.

2. METHOD

The transition or boundary region between the atomistic and continuum regions (Figure2) is the key of the modeling [5]. At the interface between the atoms and the nodes of the continuum region, we construct a one-to-one correspondence with the aid of the Chebyshev polynomials of the second kind. The polynomial Chebyshev of second kind on the interval $[-1,1]$ are given by [6-8]

$$U_n(x)=[1/(n+1)]T'_{n+1}(x),\ -1\le x\le 1,\ n\in \mathrm{N}_0. \tag{1}$$

In (1), $T_n(x)=\cos(n\arccos x)$ are the Chebyshev polynomials of the first kind, and N_0 is a set of natural numbers. The shifted Chebyshev polynomials are defined as

$$U_n^*(t)=U_n(2t-1)=\{1/[2\sqrt{t(1-t)}]\}\sin[(n+1)\arccos(2t-1)],\ 0\le t\le 1.$$

The functions

$$F^*(r,t)=1/[1+r)^2-4rt],\ h^*(x)=2\sqrt{2(1-t)},\ |r|\le 1,\ 0\le t\le 1, \tag{2}$$

are the generating and weighting functions for these polynomials .

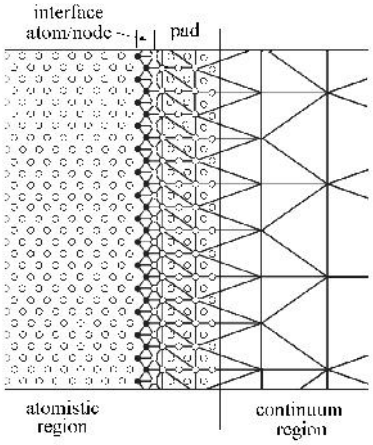

Figure 2. The atomistic/continuum transition region [6].

To obtain the basic recurrence relations, the first can be derived for $U_n(x)$ and then for $U_n^*(t)$ by substituting $2t-1,\ 0\le t\le 1$ for x. As a result, it is obtained

$$\begin{aligned} 4tU_n^*(t)&=U_{n-1}^*(t)+2U_n^*(t)+U_{n+1}^*(t),\\ 2tU_n^{*\prime}(t)&=2nU_n^*(t)+2U_{n-1}^{*\prime}(t)+U_n^{*\prime}(t),\ n\ge 1,\\ U_n^{*\prime}(t)&=4nU_{n-1}^*(t)+U_{n-2}^{*\prime}(t),\ n\ge 2. \end{aligned} \tag{3}$$

At the macrosopic, the carbon nanorope is modeled as a rod of length *l*, with circular cross section of radius less than its length $a<<l$. A new parametrization is applied to the region occupied by the body $x\in[-a,a], s\in[0,l]$, for a given time interval $t\in[0,T]$. Instead of $x\in[-a,a]$ we can use $x\in[0,1]$. For any integrable function $A(x,s), x\in[0,1],\ s\in[0,l],\ t\in[0,T]$, we consider an expansion of the form

$$A(x,s,t)=\sum_{k=0}^{\infty}A^{(k)}(s,t)\widehat{U}_k^*(x),\ \ x\in[0,1],\ s\in[0,l],\ t\in[0,T], \tag{4}$$

where $A^{(k)}(s,t)$ is the *k*th coefficient in the expansion of $A(x,s,t)$ in the orthonormal Chebyshev polynomials $\{\widehat{U}_k^*(x)\}_{k=0}^{\infty}$ of the second kind. Let us to consider the integral

$$I^{(k)}(A)=\int_0^1 A(x,s,t)\widehat{U}_k^*(x)h(x)\mathrm{d}x,\quad k\in \mathrm{N}_0\ s\in[0,l], \tag{5}$$

Where $h(s)$ is a properly chosen weighting function. This integral verifies the property of linearity

$$I^{(k)}[\alpha(s)A+\beta(s)B]=\alpha(s)I^k(A)+\beta(s)I^k(B), \tag{6}$$

for any functions A and B of the form (4). Also, it is easily to show that $I^{(k)}(A)$ is equal to the *k*th coefficient in the expansion of A in these polynomials with respect to x

$$I^{(k)}(A)=\int_0^1 A(x,s,t)\widehat{U}_k^*(x)h(x)\mathrm{d}x=A^{(k)}(s,t)\text{, with } k\in \mathrm{N}_0\text{.} \tag{7}$$

The external moments fix the ends of the tube. We suppose the rope deforms by bending and torsion. At the macroscopic scale, the motion of the rod between $t=0$ and r_{ij} is known from the given mapping

$$S(0,t),\ \forall t\in[0,t_1], \tag{8}$$

which takes a material point in the initial domain at $t=0$ to a spatial position at $t=t_1$.

We take s to be the coordinate along the central line of the natural state. The orthonormal basis of the Lagrange coordinate system is denoted by (e_1,e_2,e_3), and the orthonormal basis of the Euler coordinate system by (d_1,d_2,d_3). The basis $\{d_k\}$, $k=1,2,3$ is related to $\{e_k\}$, $k=1,2,3$ by the Euler angles θ,ψ and φ. These angles determine the orientation of the Euler axes relative to the Lagrange axes. The curvature C, in the longitudinal direction, the nondimensional curvature c, the deformation parameter ζ, are defined by

$$C=\frac{2ch}{\sqrt{3}R^2(1-\nu^2)},\quad c=\frac{\sqrt{3\zeta}}{2},\ \zeta=\frac{R-R_c}{R}, \tag{9}$$

where R and R_c, are the radius before and after deformation.

The energy field $E^{tr}(x,s)$ of the transition region verifies the conditions

$$E^{tr}(x,s)\to E^c(x,s)\text{ for } x_{tr}\to x_c,\ s_{tr}\to s_c \tag{10}$$

and

$$E^{tr}(x,s)\to E^a(x,s)\text{ for } x_{tr}\to x_a,\ s_{tr}\to s_a, \tag{11}$$

where

$$E^{tr}(x,s)=\sum_{k=0}^{\infty}E^{tr(k)}(s)\widehat{U}_k^*(x), \tag{12}$$

with $x_{tr}\in[0,1]$, $s_{tr}\in[0,l]$. In (12) $E^{tr(k)}(s)$ is the kth coefficient in the expansion of $E^{tr}(x,s)$ in the orthonormal Chebyshev polynomials $\{\widehat{U}_k^*(x)\}_{k=0}^{\infty}$ of the second kind. These coefficients can be calculated as

$$E^{(k)tr}(s)\to\int_0^1 E^a(x,s)\widehat{U}_k^*(x)h_a(x)\mathrm{d}x,\ k\in\mathrm{N}_0\text{, for } x_{tr}\to x_a,\ s_{tr}\to s_a,$$

and

$$E^{(k)tr}(s)\to\int_0^1 E^c(x,s)\widehat{U}_k^*(x)h_c(x)\mathrm{d}x,\ k\in\mathrm{N}_0\text{, for } x_{tr}\to x_c,\ s_{tr}\to s_c,$$

with unknown functions $h_a(x)$ and $h_c(x)$ that are determined from an inverse problem such that (10) and (11) hold.

The total potential energy of the coupled atomistic-continuum model is obtained by summing the energies associated with the atomistic, continuum and transition regions as

$$\begin{aligned}E(x,s)=E^c(x_c,s_c)+E^a(x_a,s_a)+E^{tr}(x_{tr},s_{tr}),\ (x_c,s_c)\in I_c,\ (x_a,s_a)\in I_a,\\ (x_{tr},s_{tr})\in I_{tr}\\ I_c\cup I_a\cup I_{tr}=[0,1]\times[0,l],\ I_i\cap I_j=O,\ i,j=a,c,tr.\end{aligned} \tag{13}$$

3. RESULTS AND CONCLUSIONS

The matrix resolution is important for the quality of the results [9-12]. There are some techniques to create the perception of depth such as active or passive stereo [9]. The use of active and passive actuators together could make possible to simulate various virtual environments with the stable, realistic illusion [10, 11].

The tool that changes the structure is a sphere. Before the compression the interface is represented in Figure 3. Figure 4 shows different cross sections of the nanorope segments for different values of ζ after compression.

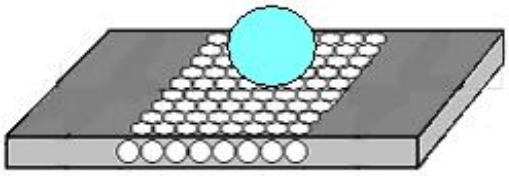

Figure 3. The interface before the compression.

The haptic feedback is calculated from the depth of the indentation of the sphere into the interface and from the neighboring field. The perturbed surface normal n_p and the gradient of the cells height ∇h are given by

$$n_p - n = (\nabla h \cdot n)n - \nabla h \,, \qquad (14)$$

where n is the original normal.

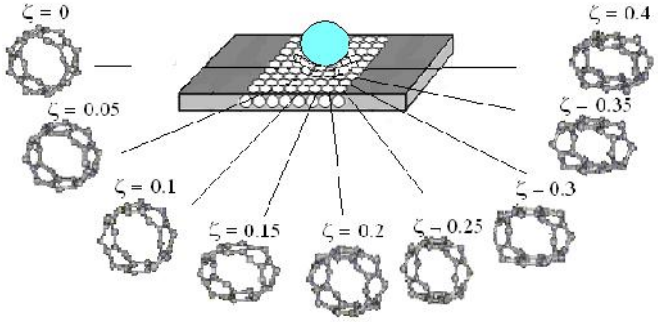

Figure 4. The interface after the compression

The calculations were carried for a sonic plate of length $l = 18\text{cm}$ and width $d = 2\text{cm}$, whith the scatterers made of carbon nanotube rope segments.

The first observed thing is that the macroscopic modeling is valid up to the point of local buckling at $\vartheta = 25.58^\circ$. For larger angles, the equation must be coupled with an atomistic theory. When the external bending moment increases, the axial compression in the tube increases too, and when the compressive stress reaches a critical value, the tube will locally buckle. The value of ζ given by (9) at the point of local buckling is around 0.14.

With the increase in the bending angle ϑ, the top and bottom parts of the kink get closer to each other, and at a certain stage, the distance between them reaches the critical equilibrium distance. Upon additional bending, this distance remains unchanged because there are no external normal loads applied on the walls to prevail over the repulsive van der Waals forces.

For $\vartheta > 25.58^\circ$, the atomistic theory put into evidence a region in which a specific mechanism of deformation appears.

The guided waves are accompanied by evanescent waves which extend to the periodic array of the scatterers surrounding the wave-guide. It is strongly expected that mode coupling waves arise between adjacent wave-guides. The output of the coupled modes is compared with the input waves, as shown in Figure5 for $\zeta = 0.35$. The remarkable result is that the ratio of the coupled and input waves is −3 to −4 dB around the frequency of 7kHz to 7.8kHz in the band-gap of the sonic material.

The visualization shows that a portion of the wall flattens and forms a domain that rotates about a central hinge line. The nanotube becomes a mechanism and the macroscopic modeling is no longer valid in this domain. The major advances in haptics and dynamic contacts can be found in [13, 14].

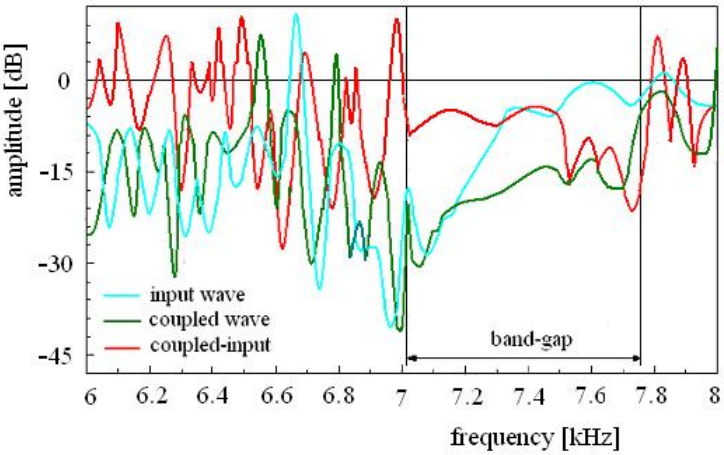

Figure 5. The input and coupled waves for sonic composite.

ACKNOLEDGEMENT

This research was elaborated through the PN-II-PT-PCCA-2011-3.1-0190 Project of the National Authority for Scientific Research (ANCS, UEFISCSU), Romania.

REFERENCES

[1] Munteanu, L., *Nanocomposites*, Editura Academiei, 2012.
[2] Chiroiu, V., Munteanu, L., V.P.Paun, P.P.Teodorescu, *On the bending and torsion of carbon nanotubes ropes* New Applications of Micro-and Nanotechnologies, Series of Micro and Nanoengineering, vol.14, 26-44, Publishing House of the Romanian Academy (eds. M.Zaharescu, M.Ciurea, I.Kleps, D.Dascalu) 2009.
[3] Chiroiu, V., Brisan, C., Donescu, St., Munteanu, L., *On the material visualization system with haptic feedback,* International Semiconductor Conference- CAS 2012, Sinaia, 2012.
[4] Dorjgotov, E., Beneš, B., Madhavan, K., *An immersive granular material visualization system with haptic feedback*, in Theory and Practice of Computer Graphics (Ik Soo Lim and David Duce (eds.) 2007
[5] Curtin, W.A., Miller, F., *Atomistic/continuum coupling in computational material science*, Modelling and Simulation in Materials Science and Engineering, 11, R33–R68, 2003.
[6] Nikabadze, M.U., *A system of equations of the thin-body theory*, Vestn. Mosk. Univ., Ser.1: Mat.Mekh., 1, 30–35, 2006.
[7] Nikabadze, M.U., *Application of Chebyshev polynomials to the theory of thin bodies*, Moscow University Mechanics Bulletin, 62(5), 56–63, 2007.
[8] Nikabadze, M.U., *The unit tensors of second and fourth ranks under a new parametrization of a shell space*, Vestn. Mosk. Univ., Ser.1: Mat.Mekh., 6, 25–28, 2000.
[9] Munteanu, L., Brisan, C., Donescu, St., Chiroiu, V., *On the compression viewed as a geometric transformation*, CMC: Computers, Materials & Continua, 2012 (in press).
[10] Evans, K.E., Alderson, A., *Auxetic materials: Functional materials and structures from lateral thinking*, Advanced materials, 12(9), pp.617–628, 2000.
[11] Brisan, C., Csiszar, A., *Computation and Analysis of the Workspace of a Reconfigurable Parallel Robotic System,* Mechanism and Machine Theory journal, vol.46, pp.1647–1668, 2011.
[12] Pacurari, R., Csizar, A., Brisan**, C.**, *Basic aspects concerning modular design of reconfigurable parallel manipulators for assembly tasks at nanoscale*, Mechanika*,* 2(76), pp.69–76, 2009.
[13] Srinivasan, M.A., Basdogan, C., *Haptic in virtual environments taxonomy, research status, and challenges,* Comput. & Graphics, vol.21, no.4, pp.393–404, 1997.
[14] Gilardi, G., Sharf, I., *Literature survey of contact dynamics modeling*, Mechanism and Machine Theory, vol.37, pp.1213–1239, 2002.